ChemistrySelect

ChemistrySelect
Chemistry Europe
European Chemical Societies Publishing

RESEARCH ARTICLE OPEN ACCESS

Ensemble Docking of FDA-Approved and Peruvian Phytochemicals Against Monkeypox Virus Telomere-Binding Protein

Edinson Gervacio-Villarreal[1] | Georcki Ropón-Palacios[1] | Claudina Sancho[2] | Jhon Pérez-Silva[1] | Kewin Otazu[1] | Gustavo E. Olivos-Ramirez[3] | Karolyn Vega-Chozo[1] | Yaritza L. Ramirez-Díaz[1] | Manuel E. Chenet-Zuta[4] | Ivonne Navarro del Aguila[5] | Mario De la Cruz Flores[5] | Cinthia Aguiar[1] | Ihosvany Camps[1]

[1]Laboratório de Modelagem Computacional - LaModel, Instituto de Ciências Exatas - ICEx, Universidade Federal de Alfenas - UNIFAL-MG, Minas Gerais, Brazil | [2]Universidad Peruana Cayetano Heredia, Lima, Perú | [3]Department of Biosystems and Soft Matter, Institute of Fundamental Technological Research, Polish Academy of Sciences, Warsaw, Poland | [4]Universidad Nacional Tecnológica de Lima Sur UNTELS, Lima, Perú | [5]Universidad Nacional de la Amazonía Peruana, Iquitos, Perú

Correspondence: Georcki Ropón-Palacios (groponp@gmail.com) | Ihosvany Camps (icamps@unifal-mg.edu.br)

Received: 18 July 2025 | **Revised:** 8 December 2025 | **Accepted:** 28 January 2026

Keywords: drug screening | ensemble docking | Monkeypox virus | telomere binding protein

ABSTRACT

Monkeypox is a reemerging zoonotic disease that has been spreading worldwide. Different approaches are being conducted to find effective treatments for this disease. To accelerate therapeutic discovery, we propose telomere-binding protein (TBP) as a potential drug target because of its important role during virus maturation. Using computational biology and biophysics techniques, the MPXV TBP was modeled, and a library of FDA-approved drugs and phytocompounds was screened using a rigorous ensemble docking protocol; conformational sampling was enhanced by enumerating, for each ligand, ionization states, tautomerism, and ring conformations. Our results present a new approach to drug selection against MPXV, with six potential inhibitors: CHEMBL3894860, CHEMBL461101, CHEMBL2103870, PNSC125, PNSC305, and PNSC123, which can be taken as lead compounds for experimental testing, for example, in plaque reduction assays and qPCR in MPXV-infected cells to determine EC50, CC50, and selectivity index (SI) values.

1 | Introduction

Monkeypox is a reemerging zoonotic viral disease caused by the Orthopoxvirus *Monkeypox virus* (MPXV) [1, 2]. According to the World Health Organization (WHO), between January 2022 and November 2023, 92,783 cases of MPXV were reported, with 171 deaths, in 116 countries [3]. Historically, outbreaks outside Africa were uncommon, with notable events such as the 2003 episode in the United States and other countries [3–5]. However, recent reports have described cases with no links to enzootic regions or animal exposure, suggesting changes in the observed transmission patterns [6–8]. In 2024, the WHO documented 1854 confirmed cases in the African Region, representing 36% of global cases, along with more than 15,000 clinically compatible cases and over 500 deaths in the Democratic Republic of the Congo, exceeding the figures reported in 2023 [2]. Additionally, the Ib subtype has shown predominantly human-to-human transmission and has been reported in countries with no prior documentation of the disease, including Burundi, Kenya, Rwanda, and Uganda [2, 9]. Taken together, these ongoing shifts in the epidemiological landscape of MPXV, along with its recent geographic expansion, position the virus as an increasing threat to global health and underscore the need to identify new antiviral targets.

MPXV is analogous to smallpox, caused by the smallpox virus (VARV), which occurs only in humans [10, 11]. Both have similar morphology, size, and genome (96.7%) [12]; however, MPXV has a wide range of hosts, making it capable of infecting various species, such as rodents, monkeys, and humans [13, 14]. According to the WHO, virus transmission has been particularly notable among bisexual and homosexual men and presents greater risks for immunocompromised individuals [3, 15–17]. Although the possibility of respiratory transmission has been observed in animal studies, this mode of transmission is considered less likely [18]. Studies have already reported the presence of MPXV in body fluids such as saliva, semen, urine, and feces [19], indicating greater complexity in infection pathways and the need for surveillance.

Currently, sequencing shows two clades of MPXV: the Central African (CA) clade, which is more lethal, with a fatality rate of (10.6%), compared to the West African (WA) clade, which presents (3.6%) [20, 21]. Additionally, 46 relevant mutational differences have been reported between the strains from the 2018 and 2024 outbreaks, and others have considered them SNPs (single nucleotide polymorphisms) [22–24]. Furthermore, the mutations accumulated during the 2022 outbreak exceeded the previously estimated substitution rates for Orthopoxvirus [22, 23]. This increase is consistent with the action of human APOBEC3 enzymes, which generate transitions characterized by cytosine conversion in the viral genome [24–26]. Taken together, these findings suggest a lineage rapidly adapting to the human host, with direct implications for the evolution, genomic surveillance, and epidemiological risk of MPXV.

Despite its spread and increasing risk, to date, there are no vaccines or specific medications approved specifically against MPXV [27]. However, it is known that the smallpox vaccine provides approximately (85%) protection against MPXV [28, 29], which is likely due to cross-reactivity [30]. Regarding antivirals, to date, the FDA has only approved drugs for other viruses of the Orthopoxvirus genus, such as: cidofovir, a viral DNA polymerase inhibitor with renal cytotoxicity; brincidofovir, which targets viral DNA polymerase; nitoxantrone, involved in the final stage of virus assembly; and tecovirimat, a VP37 protein inhibitor [31–35]. These drugs are under investigation, as they are not specific to MPXV [36]. Furthermore, cases of tecovirimat resistance have been reported in immunocompromised patients due to mutations in F13 [37–40]. These limitations highlight the need to identify therapeutic targets that act at essential stages of the replicative cycle and avoid cross-resistance.

During the maturation of the virion, the synthesized DNA must be packaged, a process assisted by an ATPase and a protein that binds to viral telomeres [41]. Telomere-binding proteins (TBP) bind directly and specifically to double-stranded TTAGGG telomeric repeats, and their domain structure is similar [42]. The TBP protein is known for its role in the regulation of telomerase, thus controlling telomere length, and plays a crucial role in protecting the ends of chromosomes [43, 44]. The MPXV genome encodes TBP that is conserved in the genus Orthophoxvirus [45]. TBP-MPXV, also known as an essential virosomal protein for virus multiplication, is a late expression protein (Late) I1L [46]. As its telomere binding name implies, I1L binds to the S-hairpins of the virus telomeres [47]. This protein has 312 amino acids and is encoded by the conserved central region of the genome [23, 48]. In vitro studies on Vaccinia virus (VAC) indicate that it plays an important role in genome packaging and is required for the production of mature virions [47, 49]. Its suppression leads to an accumulation of immature virions [47], which prevents viral assembly and dissemination. Given its essential role in viral maturation and its structural conservation, TBP-MPXV represents a highly attractive and as yet unexplored therapeutic target.

Unlike the available antivirals, which primarily target F13/VP37 or the viral DNA polymerase, inhibition of TBP orthogonally disrupts genome packaging and virion maturation, creating a critical bottleneck in the replicative cycle [39, 50]. This strategy is particularly relevant given reports of tecovirimat resistance in immunocompromised patients, associated with multiple F13 mutations that alter trimer stability [37–39]. Furthermore, the high conservation of the Myb domain involved in DNA binding, together with its low identity (1%–18%) relative to human Myb-type proteins, suggests the potential for broad-spectrum antiviral activity with a favorable selectivity profile, reducing off-target risks compared with cidofovir or brincidofovir [51–53].

MPXV TBP demonstrates remarkable sequence identity exceeding 85% with both VACV I1L and variola virus TBP within the critical Myb domain, particularly in the H1–H3 helices that mediate DNA binding [51, 52]. This structural conservation extends to the druggable tunnel-like pocket and essential residues including R137 and R198 [51, 52], suggesting that inhibitors designed against MPXV TBP may retain efficacy across multiple Orthopoxvirus species. Given this degree of conservation, we propose that small molecules capable of achieving comparable binding affinities between TBP orthologs, such as VACV I1L(PDB:2VSL) and MPXV TBP, could support the development of pan-Orthopoxvirus antivirals suited to counter emerging variants and enable unified therapeutic strategies. In contrast to this strong viral conservation, human Myb family proteins (c-Myb, A-Myb, B-Myb) share only 1%–18% identity with viral TBPs and display distinctive KDKXR motifs, as well as divergent charge distributions and loop-region variations between viral and human Myb-type proteins [47]. These structural differences support the possibility of selective targeting of viral TBP. Moreover, target-prediction studies based on chemical similarity, such as SEA and SwissTargetPrediction, have demonstrated their utility in evaluating potential human off-targets [54]; in this context, the absence of predicted affinity toward human Myb-type proteins suggests a reduced likelihood of human protein interference and further reinforces TBP as a selective antiviral target within Orthopoxvirus.

The absence of crystallographic or cryo-EM structures of MPXV TBP, combined with the experimental challenges of studying essential Orthopoxvirus proteins, has driven the adoption of computational approaches such as structural modeling, molecular dynamics, and ensemble docking—tools that are critical for accelerating antiviral discovery in emerging or re-emerging pathogens with limited experimental data. Because TBP exhibits conformational dynamism and multiple functional states, ensemble docking enables a more realistic assessment of binding-site flexibility and facilitates the prioritization of inhibitors with a higher likelihood of targeting biologically relevant structural states.

Given the lack of MPXV-specific antivirals and the urgent need to identify virus-encoded therapeutic targets, we evaluated MPXV TBP as a potential drug target. Building on the structural and dynamic characterization described above, we conducted an extensive virtual screening of FDA-approved compounds and Peruvian phytochemicals to identify lead molecules suitable for future experimental validation.

2 | Materials and Methods

2.1 | Library of Chemical Compounds Generation

A library of chemical compounds was prepared to investigate the pharmacological capacity of TBP-MPXV by ensemble docking. First, FDA-approved drugs obtained from the ChEMBL database [55] and phytocompounds extracted from Peruvian medicinal plants were collected. Both sets of compounds were initially in SMILES format. Subsequently, they were converted to SDF and PDB formats using the GypsumDL tool [56, 57]. This conversion was performed with a pH range of 7.4–8.4, generating five conformers for each ligand. Then, the Durrant filter, implemented in GypsumDL [56] was applied to eliminate conformers. Technically possible but considered unlikely, these filters were performed with the flag `--use_durrant_lab_filters`, which exclude molecular variants containing chemically improbable or unstable substructures. These include, among others, species such as `C = [N-]`, `[N-]C = [N+]`, `[nH+]c[n-]`, `[#7+]~[#7+]`, `[#7-]~[#7-]`, `[!#7]~[#7+]~[#7-]~[!#7]`, boron-containing moieties (`[#5]`), `O = [PH](= O)([#8])([#8])`, `N = c1cc[#7]c[#7]1`, and `[$([NX2H1]),$([NX3H2])] = C[$([OH]),$([O-])]`, as well as compounds containing metals. These filters ensure the exclusion of chemically implausible structures that could interfere with downstream virtual screening and docking analyses. After applying the Durrant filtering criteria, the phytochemical dataset comprised 324 unique molecules and 1202 corresponding 3D conformers, whereas the FDA-approved compounds resulted in 1583 unique molecules and 5104 conformers. Finally, the resulting PDB files were converted to PDBQT format using the prepare_ligand.py tool in AutoDockTools [58] resulting in 5601 and 1415 conformers from FDA drugs and Peruvian phytocompounds, respectively.

The selection of Peruvian medicinal plants for antiviral research is grounded in centuries of ethnopharmacological practice and increasingly substantiated by contemporary scientific evidence. Peru's medicinal plant legacy—encompassing over 22,000 plant species with exceptional endemism—provides a rich repository for drug discovery, particularly within traditional contexts treating respiratory infections, coughs, and fever-related conditions that often have viral etiologies. The ethnopharmacological approach, validated by the ICBG-Peru project and extensive ethnobotanical surveys documenting medicinal use among indigenous communities from the Amazonian Cashinahua to Asháninka peoples, serves as a rational framework for plant selection. During the COVID-19 pandemic, 80.2% of surveyed Peruvian populations used medicinal plants for prevention, with eucalyptus, ginger, garlic, and matico leading as preferred treatments for respiratory symptoms—indicating both cultural significance and pragmatic application of these species in managing infectious respiratory diseases. This demonstrated therapeutic engagement with traditional plant knowledge reflects cumulative centuries of observation rather than arbitrary selection, providing a legitimate ethnobotanical basis for investigating their antiviral potential [59–61].

The antiviral rationale for specific Peruvian plants is now well-documented through rigorous experimental validation. Uncaria tomentosa (Cat's Claw) demonstrates potent mechanisms against viral infection, including pentacyclic oxindole alkaloids and polyphenolic compounds that block SARS-CoV-2 spike protein interaction with ACE-2 receptors (binding affinity ranging from −6.0 to −8.6 kcal mol^{-1}), with in vitro efficacy against dengue virus, herpes simplex virus type 1, and multiple enveloped viruses. Piper aduncum (Matico), traditionally used for respiratory conditions, and medicinal species like Schinus molle possess antimicrobial and anti-inflammatory properties documented through conventional phytochemical analysis and molecular docking studies against SARS-CoV-2 protease targets. Recent in silico screening identified polyphenolic compounds from Peruvian plants—including rutin from traditional remedies—exhibiting binding scores comparable to or exceeding approved antivirals like remdesivir and lopinavir against viral protease and polymerase targets. These plants are distinguished not by novelty alone, but by the synthesis of traditional ethnopharmacological use, demonstrated biological activity, and mechanistic understanding of their bioactive compounds against recognized viral targets—a convergence that reflects genuine therapeutic rationale rather than speculative selection [62–66].

2.2 | Modeling

The TBP-MPXV amino acid sequence was retrieved from UniProt Q8V518 [67]. Then, its 3D structure was modeled using AlphaFold v2, this advanced artificial intelligence software determines the three-dimensional conformation of the protein from the primary sequence and an extensive database of crystallographic structures [68]. To this process, we employed all generic CASP14 databases, updated as of May 14, 2020, in full_dbs mode. Our model produced 19 PDB hits of crystallographic proteins used as templates (Table S1). We performed the predicted Local Distance Difference Test (pLDDT) to evaluate the reliability of the model. In addition, we aligned TBP sequences from several cell lines (Table S2) using the MSA package [69] in R [70] to confirm that the target protein is not homologous to human TBP and to verify the conservativeness of the Myb motif.

2.3 | System Settings

The model generated by AlphaFold v2 was protonated at pH 7.0 with the PDB2PQR tool [71]. The CHARMM-GUI server [72] was used to create the system topology and add water molecules from the TIP3P model [73] inside a 15 Å cubic box. The system was then neutralized with Cl^- and Na^+ ions at a concentration of 0.150 M to simulate the physiological conditions of a biological environment.

2.4 | Molecular Dynamics Simulations

Minimization, equilibration and production were performed using GROMACS v2021.3 software [74]. Initially, the system was

energetically minimized with 50,000 steps to reach an energy below 1000 kJ mol^{-1} nm^{-1}. Subsequently, equilibration was performed in two stages: first, temperature equilibration with a canonical set (NVT) at 310 K for 2 ns using the Berendsen algorithm [75], and second, pressure equilibration with a Gibbs set (NpT) at 1 bar for 5 ns using the Parrinello–Rahman barostat [76]. In both stages, the backbone and side chains were restrained with a constant force of 400 and 40 kJ mol^{-1} nm^{-2}, respectively.

Finally, the production of the trajectories ran out for 100 ns using the leap-frog integration algorithm. To constrain hydrogen bonds to heavy atoms, the LINCS algorithm [77] was employed. For hydrogen bonds in water molecules, the SETTLE algorithm [78] was used. Non-bonded interactions were treated using a cutoff scheme and the split-mesh Ewald method (PME) [79] to calculate the short- and long-range interaction, respectively.

2.5 | Ensemble Generation

Molecular dynamics trajectories of TBP-MPXV were clustered using the GROMOS algorithm [80] through the gmx clustering module, using RMSD cutoff values of 0.2, 0.3, 0.4, and 0.5 nm. Subsequently, the five most representative conformations of each cutoff value were selected, obtaining a total of 20 clusters for further analysis, it is said that this set of clusters constitutes an ensemble.

2.6 | Evaluation of the Pharmacological Capacity of TBP-MPXV

The 7016 conformers were docked against the 20 ensemble clusters using AutoDock Vina v1.1.2 [81] with the following configuration: the grid box was centered at $(x, y, z) = (0.237, 0.040, -0.159)$ Å and had dimensions $70 \times 74 \times 56$ Å (along x, y, z, respectively), as determined by a TCL script (`get_box.tcl`); the grid spacing was set to 1.0 Å and `exhaustiveness` to 28. For each conformer (FDA or phytocomposite), an average ensemble score [82] was then computed as follows:

$$\bar{\mathbf{E}} = \frac{\sum_{i=1}^{20} \mathbf{W_i E_i}}{\sum_{i=1}^{20} \mathbf{W_i}} \tag{1}$$

$\bar{\mathbf{E}}$ is the weighted average ensemble score, $\mathbf{W_i}$ is the size of cluster $\mathbf{i}$ (number of conformers composing the cluster), and $\mathbf{E_i}$ is the binding energy of the conformomer attached to cluster $\mathbf{i}$. The purpose of this equation is to generate a score to identify the top 10 conformomers. Then, the Boltzmann equation was applied to each of these conformers bound to cluster $\mathbf{i}$ to determine the 10 complexes most likely to form. First, we defined the partition function $\mathbf{Z}$:

$$\mathbf{Z} = \frac{\mathbf{1}}{\sum_{i=1}^{20} \mathbf{e}^{-(E_i/k_B T)}}. \tag{2}$$

Then, we calculate $\bar{\mathbf{B}}_\mathbf{i}$:

$$\bar{\mathbf{B}}_\mathbf{i} = \mathbf{Z}\mathbf{e}^{-(E_i/k_B T)} \tag{3}$$

$\bar{\mathbf{B}}_\mathbf{i}$ is the probability of the conformomer to bind to cluster $\mathbf{i}$, $\mathbf{E_i}$ is the binding energy of the conformomer attached to cluster $\mathbf{i}$, $\mathbf{k_B}$ is the Boltzmann constant in kcal mol^{-1} K^{-1}, and T is set to 298 K. Once the top 10 complexes were determined according to drug origin, we analyzed their interactions with PLIP v2.2.2 [83].

2.7 | Molecular Data Analysis

We performed a statistical analysis for the results of the interaction energies for each generated ensemble to determine that our approach leads to better drug-receptor interaction with statistical significance. This approach improves recovery of any ligand that may be lost in simple docking. To achieve this, we first determined the data distribution using the Kolmogorov–Smirnov test. Subsequently, using the Kruskal–Wallis test, we determined the existence of statistical differences in the groups (the ensembles within each RMSD clustering) and then we established the difference between each group with the Holm–Bonferroni post hoc test. This pipeline was performed using the ggstatsplot [84] library in R [70]. The images were generated with VMD v1.9.4 through an in-house Tcl script suite, while the plots were generated in R with the ggplot2 v3.4.4 [85] and ggstatsplot [84] packages. The trajectories were analyzed with an in-house Python script suite based on the MDAnalysis v2.0 library. Finally, the secondary structures were calculated with DSSP through GROMACS v 2021.3 [74]. ADMET analysis was performed for the hit compounds using the ADMETlab v2.0 tool [86]. Figure 1 illustrates the methodological workflow used in this study.

3 | Results

Computational biology and biophysics methods have been applied to study TRBF-MPXV as a potential therapeutic target. Because its tridimensional conformation has not previously been determined by experimental methods, our findings represent the first insights into the structural characteristics of this protein. Here, we present the results of structural modeling, conformational sampling, virtual screening, and molecular dynamics simulations that support the hypothesis of TRBF-MPXV druggability.

3.1 | Modeling and Sequence Alignment

In this study, we build a high-quality TBP model based on the pLDDT analysis. 57.70% of the amino acids presented a pLDDT $\geq$ 90, indicating a high accuracy of the model; 25.7% had a pLDDT between 70 and 90, which is also considered to be a good precision; only 7.76% of the amino acids presented a pLDDT between 50% and 70%, and only 8.83% of these had a pLDDT $\leq$ 50. It should be noted that low-scoring pLDDT residues are associated with the terminal regions of the protein, which is only disordered at the N-terminal of our model (Figure 2A).

After 100 ns of molecular dynamics simulations, we noticed some structural changes, mainly in the proximity from the N-terminal region, which possesses a long alpha helix. We also observed some variations in the electrostatic potential of the protein, comparing

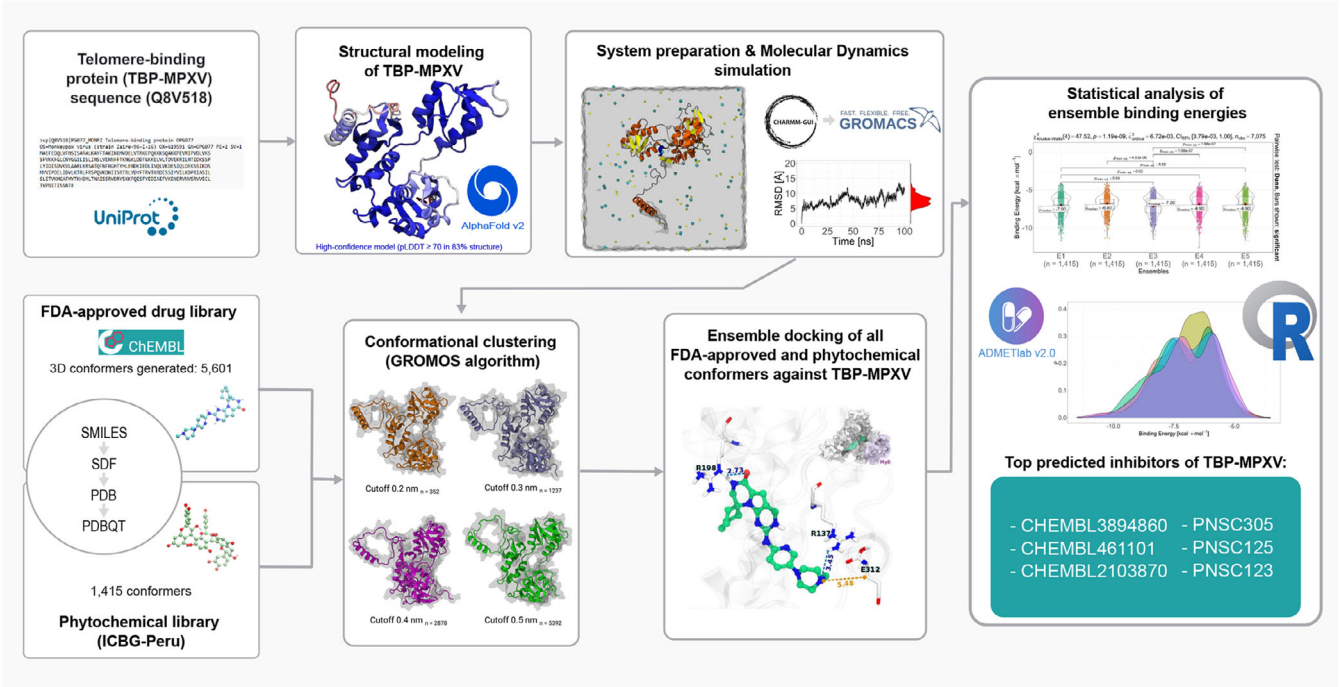

FIGURE 1 | Flowchart of the used methodology.

the initial model with the final one after molecular dynamics. Here, a change from negative to positive charge exposure is observed in the N-terminal region, while in the central region, an increase of negatively charged surfaces can be observed after molecular dynamics. It should also be noted that the Myb domain shows a conformational change where the inside oriented region becomes more negative (Figure 2B).

Moreover, we focus on the Myb domain as an important domain for DNA binding. This domain showed significant amino acid changes compared to human homologous sequences TERF1 and TERF2, of the three regions of the Myb motif, only the H_2 region is conserved by two amino acids, E275 and I281 (Figure 2C), revealing the low conservation of this region. However, our alignment analysis also revealed that the characteristic helical structures of this motif (H_1, H_2, and H_3) are maintained in the MPXV telomere-binding protein.

During the simulations at 100 ns, high fluctuations in RMSD were observed during the 100 ns of simulations (Figure 3A), corresponding to fluctuations in the N-terminal domain and Myb motif, in addition to an unpacking effect and displacement of three notable regions of the protein (Figure 3B); this possibly caused fluctuations in the solvent accessible area (SASA plot in Figure 3A) and in the radius of gyration (Figure 3A). Furthermore, observing the fluctuations of residues in the conformational space, we noticed a higher compactness in the central region and high fluctuations in the regions more exposed to the solvent (Figure 3C). Lastly, regarding the conformation of secondary structures, no notable changes were observed in the alpha helices or beta sheets, nor in the transient secondary structure formation; although we noticed the occurrence of turns (blue) and bends (yellow) in the most disordered regions (loops) (Figure 3D).

3.2 | Ensemble Generation

Our molecular modeling results guided us to use a docking assembly approach, to cope with a larger conformational cluster search and to simulate TBT in a solvent (Figure 4A). Consequently, clustering tests led us to consider four representative values (RMSD cutoff values of 0.2, 0.3, 0.4, and 0.5 nm) of which we present the most populous models of each in Figure 4B, where a larger population is observed with increasing cut-off (as expected).

3.3 | Ensemble-Guided Molecular Docking

After a thorough evaluation and weighting based on the average score of the assembly, together with the Boltzmann equation, we determine the differences by comparing the energies obtained for each of the assemblies. Our approach aims to find statistical differences between the different assemblies studied, and from there, to recover the molecular interactions that depend on the protein conformation, to recover the molecular interactions that depend on the protein's conformation. Consequently, for FDA-approved compounds and phytocompounds, a non-normal distribution in interaction energies was observed (Figure S2), which led us to use the Kruskal–Wallis test, which showed significant statistical differences ($p \leq 0.05$) between the groups, mainly for the cluster groups with 0.2, 0.4, and 0.5 nm cutoffs for the phytocompounds, as well as for the cluster groups with 0.2 and 0.3 nm cutoffs for the FDA-approved drugs.

For the 0.2 nm cutoff (Figure 5A) the E3 cluster shows the best mean interaction energies ($\mu_{median} = -7.20$) and almost all clusters of this cutoff show statistical differences. The same is true for the clusters with 0.4 nm and 0.5 nm cutoffs (Figure 5B,C), where

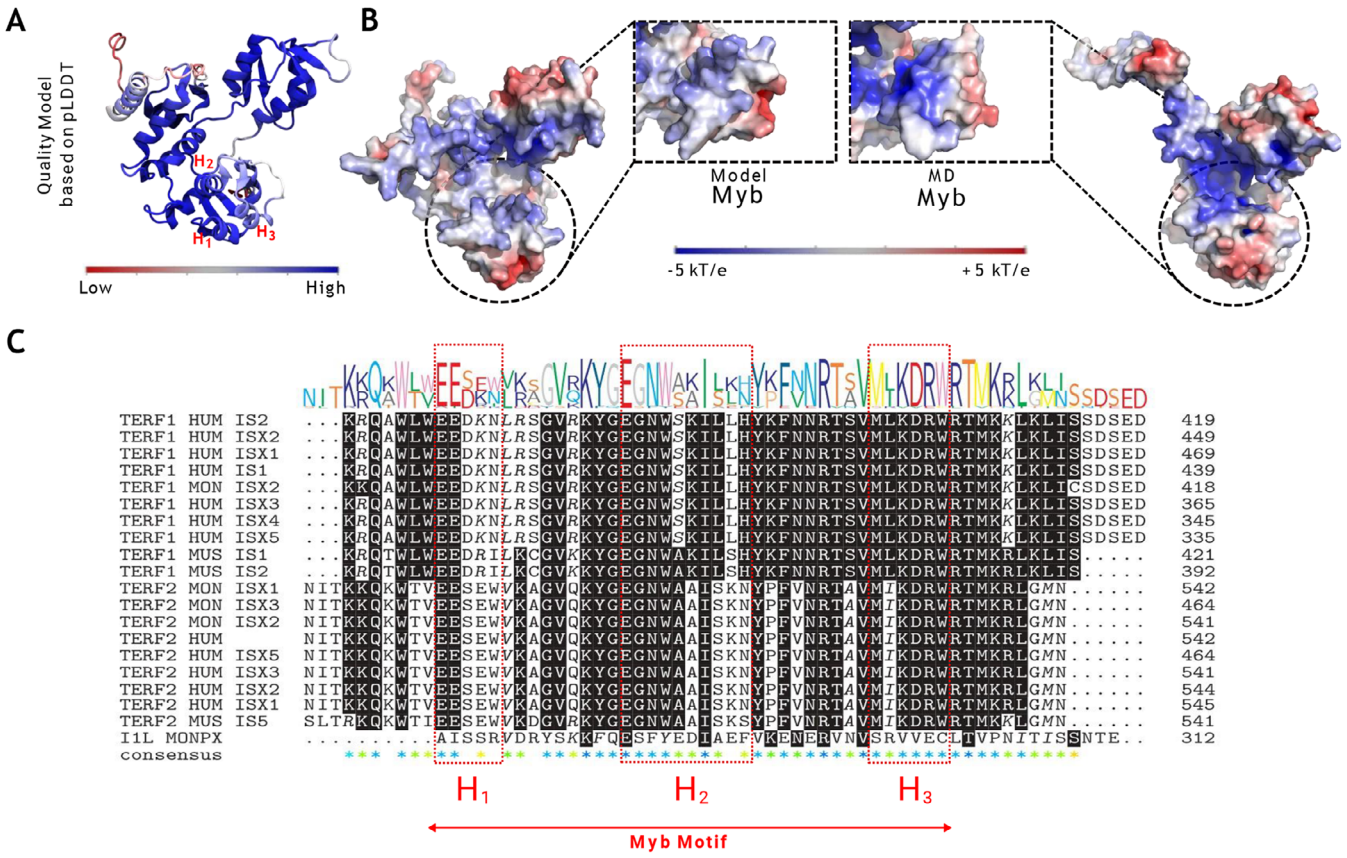

FIGURE 2 | Protein modeling, electrostatic potential and sequence alignment. (A) Telomere-binding protein model from MPXV. The residues have been colored based on the pLDDT scores (Figure S1), in which it can be appreciated that the highest accuracy of the model belongs to the folded domains and only the loops and the N-terminal regions have low reliability. (B) The model's electrostatic potential and the structure after 100 ns of molecular dynamics is shown. Here, we can appreciate changes in the exposure of positively and negatively charged regions, mainly at the N-terminal, the central region of the protein, and the Myb motif. (C) Alignment of the Myb motif that highlights the characteristics of the H_1, H_2, and H_3 regions (alpha helices) of TBP. TBP sequences in humans tend to be highly conserved, while in MPXV there is a low level of conservation. MPXV, Monkeypox virus; TBP, telomere-binding protein.

almost all sets are statistically different; moreover, the best mean energies are obtained with clusters E5 and E2, respectively. It should be noted that we only present an average energy calculated from the best interaction energies per compound corresponding to each cluster.

For FDA-approved molecules, the Holm-Bonferroni post hoc test indicates significant statistical differences ($\rho_{\text{Holm}} \leq 0.05$) for at least four of the studied clusters with a 0.2 nm cutoff (Figure 6A). We also highlight that the cluster that presented the best interaction energies was E3 ($\mu_{\text{median}} = -6.70$). On the other hand, for the 0.3 nm cutoff point, we observed statistical differences between almost all clusters. For this cluster, the best energies were observed in E2 (Figure 6B).

3.4 | TBT-MPXV Pharmacological Screening

In the distance analysis, we observed that for FDA-approved compounds, the H-bond interactions have reliable distances (between 2.01 and 3.45 Å,Table S3). Similarly, for phytocomposites, the distances of the H bonds are in the appropriate range (between 1.81 and 3.40 Å); however, we observed a greater number of these interactions (Figure 7, Table S4). This is attributed to the nature of the phytocompounds themselves and also to the different conformational and protonation states evaluated.

For the top 10 FDA-approved compounds (Table 1), the best interaction energies occurred most frequently for the groups with a cut-off of 0.3 nm. Of these, CHEMBL461101 (for which we studied three variants) presented the best interaction energy ($\Delta G \approx -10.3$ kcal · mol^{-1}). We note that although this compound exhibits the best interaction energies, the molecular interactions are different for each binding mode (variant), which leads to the interactions occurring at different sites of the protein in which the drug interacts with a larger number of residues located around the central region and at the C-terminus. CHEMBL3894860 (for which we studied four variants) was the compound that occurred the most frequently in the top 10 and also had the second-best interaction energies ($\Delta G \approx -10.1$ kcal · mol^{-1}). In contrast, this drug interacts with residues located between the central region and the N-terminal. The third molecule, CHEMBL2103870 appeared only once in our top 10, with an interaction energy similar to the other two ($\Delta G = -10.1$ kcal · mol^{-1}). Interestingly, this molecule interacts in the central region of the protein, making contacts with two loops connecting the

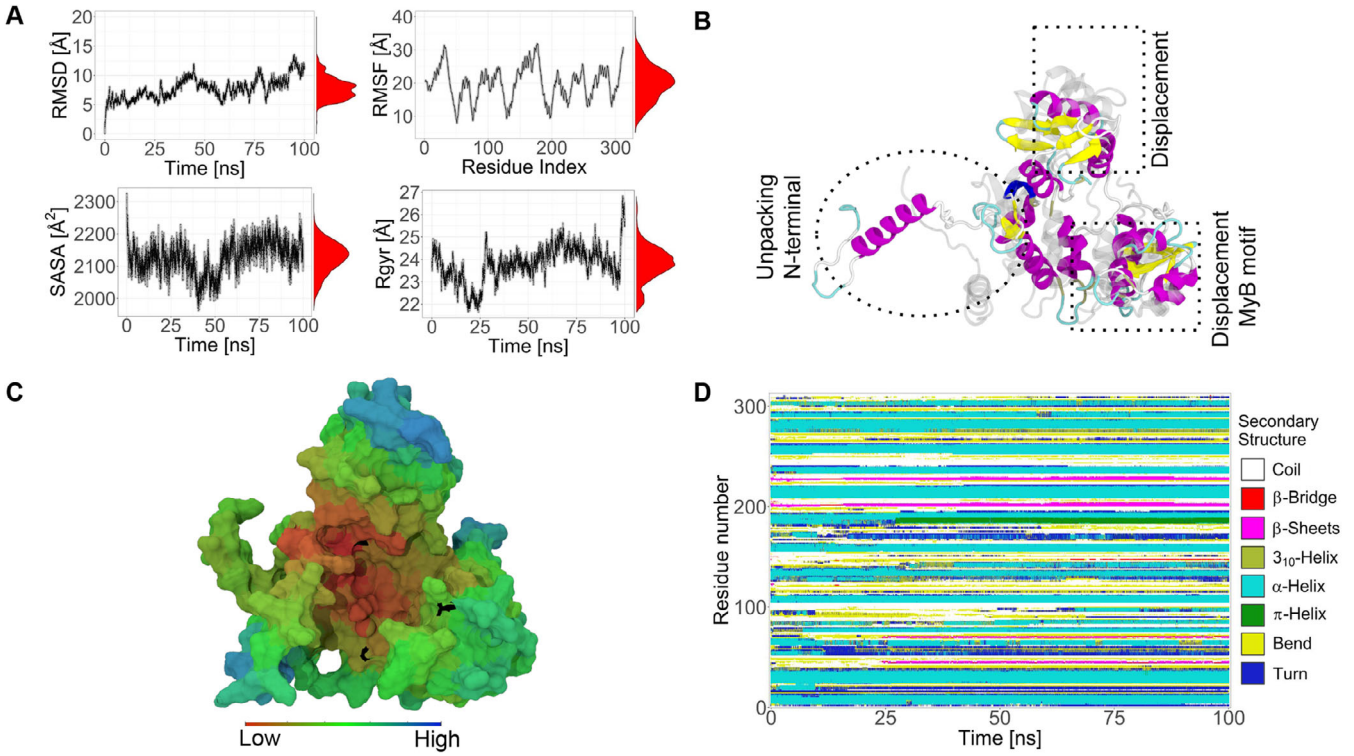

FIGURE 3 | Structural analysis of TBP-MPXV. (A) Principal stability parameters evaluated from the trajectories, the red curve represents the probability distribution of the data. The RMSDs show a conformational change of up to ≈ 14 Å with respect to the initial model, while the RMSFs show several fluctuating regions, mainly in the central regions, loop regions, and the N and C-terminus regions. Consequently, these structural changes explain the fluctuation of the SASA and the radius of gyration (Rgyr) of the protein in the lower left and right graphs of (C), respectively. (B) Comparison between the initial model (gray, back view) and the final model after molecular dynamics simulation (colored, overlay). We observed changes in the position of three important regions: the N-terminal region, which shows an unpacking effect, the Myb motif, which is displaced, and the indicated top region of the TBP, which is also displaced. (C) Representation of amino acid fluctuations in TBP colored by RMSD values. Here, we note high stability in the central region of the protein, whereas in contrast, the regions more exposed to the surface are more fluctuating. (D) We present an analysis of the conformations of secondary structures as a function of simulation time, in which we noticed that the secondary structures are maintained over time, but slight bends and turns are observed in the loop regions. MPXV, Monkeypox virus; TBP, telomere-binding protein.

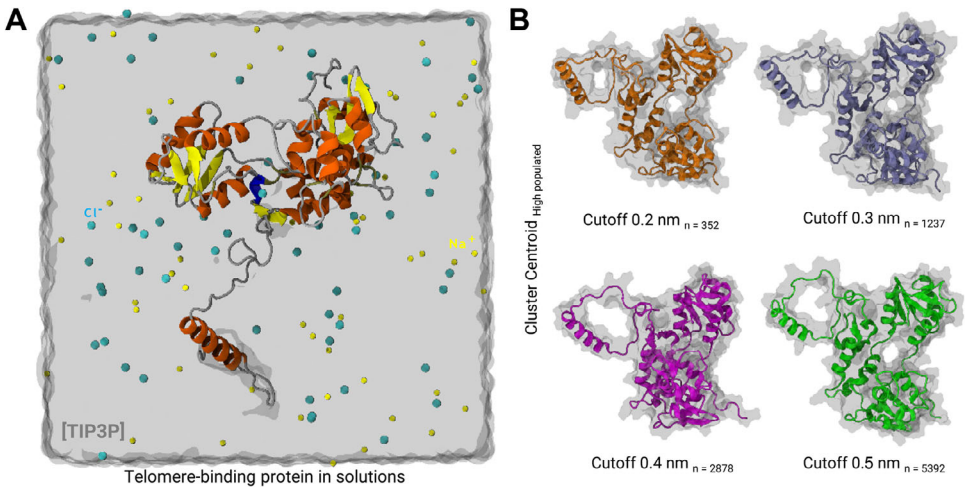

FIGURE 4 | Molecular dynamics ensembles of TBP-MPXV. (A) The TBP structure in a solvent. (B) The most populated conformations with the number of structures (*n*) of each ensemble, corresponding to RMSD cut-offs of 0.2, 0.3, 0.4, and 0.5 nm, are shown. TBP-MPXV, telomere-binding protein-Monkeypox virus.

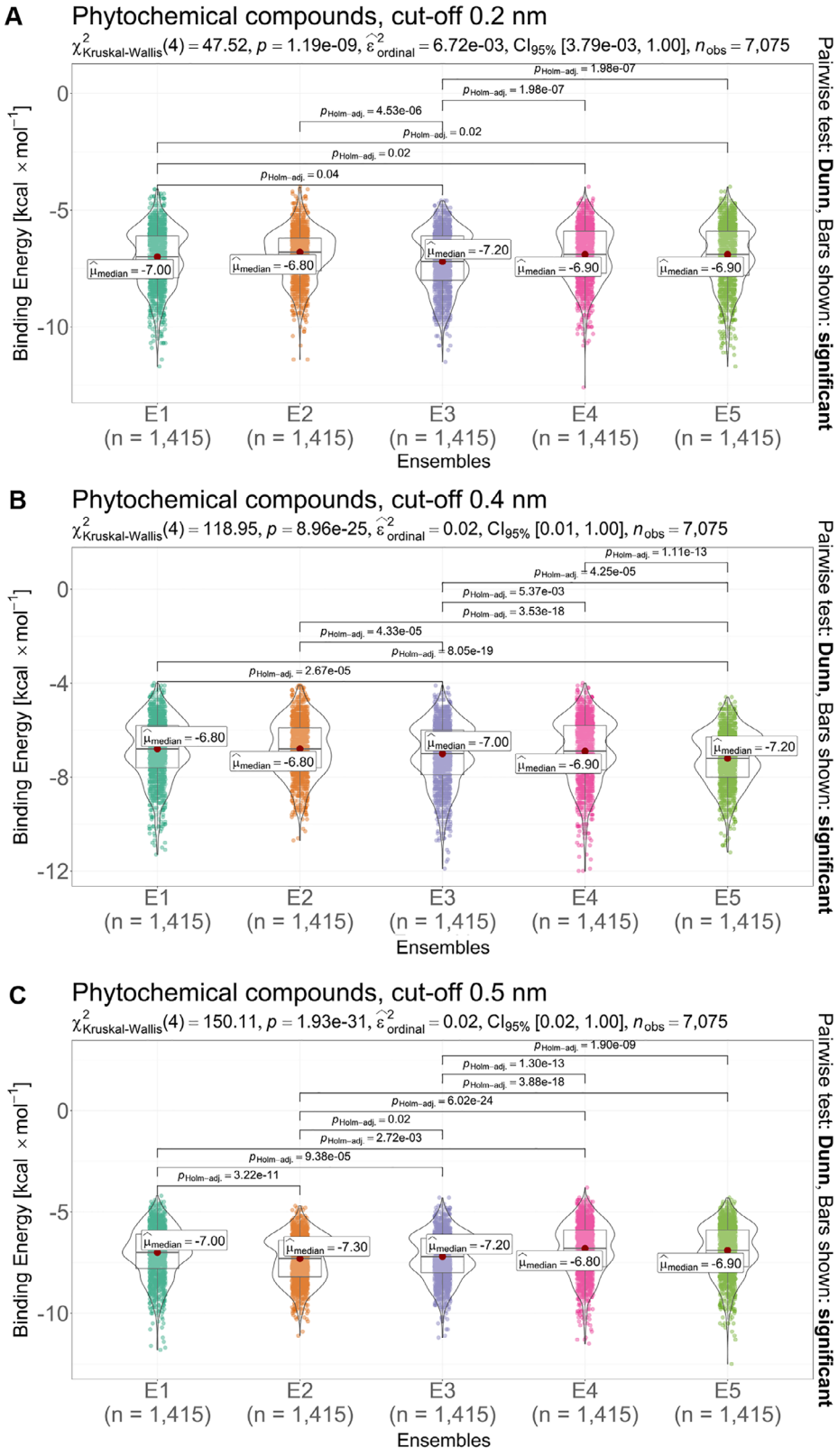

FIGURE 5 | Statistical analysis of the interaction energies obtained through ensemble docking of phytochemical compounds. (A) Kruskal–Wallis test for the 0.2 nm cut-off groups, it is observed that the E2 group is not statistically different from E1, E4, and E5, and there are no significant statistical differences between the latter two groups. (B) Kruskal–Wallis test for the 0.4 nm cut-off group. Between groups E1, E2, and E4, there are no significant statistical differences. (C) Kruskal–Wallis test for the 0.5 nm cut-off group. The group E5 is not statistically different from E1 and E4. Only $p \leq 0.5$ is shown.

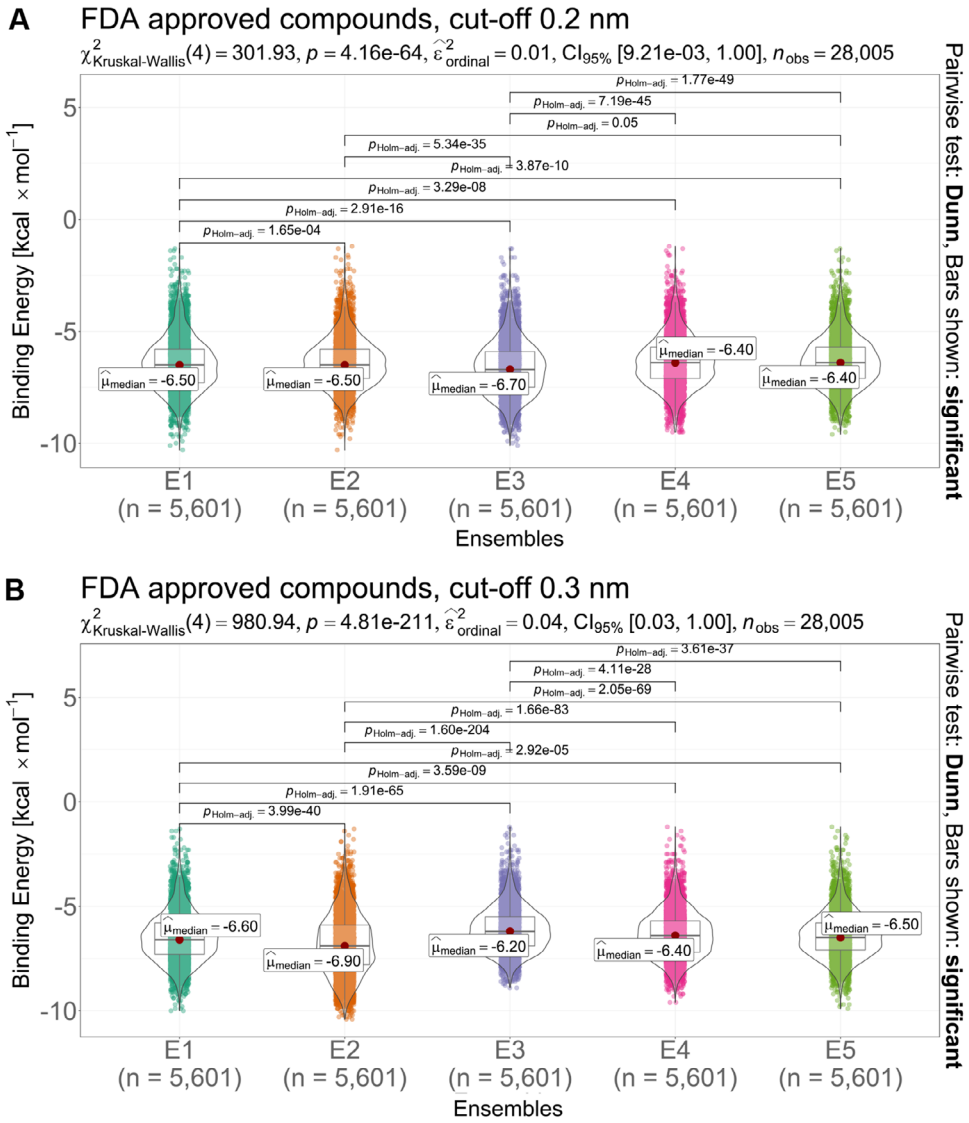

FIGURE 6 | Statistical analysis of the interaction energies obtained through ensemble docking of FDA-approved drugs. (A) Kruskal–Wallis test for the 0.2 nm cutoff group, it is observed that the E4 group is not statistically different from the E2 and E5 groups. (B) Kruskal–Wallis test for the 0.3 nm cutoff group, the E5 group is not statistically different from E4. Only $p \leq 0.5$ is shown. FDA, Food and Drug Administration.

Myb domain and the upper domain (In the upper right part of Figure 7A–C).

However, for the top 10 phytocompounds (Table 2), the best interaction energies occurred with the clusters with cut-offs of 0.2 and 0.5 nm. Here, PNSC305 (for which we studied three variants) was the compound with the highest frequency and also had high interaction energies ($\Delta G \approx -12.0\,\text{kcal} \cdot \text{mol}^{-1}$), which outperforms the energies found with the FDA-approved compounds. It should be noted that this phytocompound interacts with residues only in the central region of the protein. Although PNSC125 (for which we studied two variants) had a higher affinity ($\Delta G \approx -12.6\,\text{kcal} \cdot \text{mol}^{-1}$); however, the interactions of this compound occur with residues close to the N-terminal region of the protein. A similar interaction energy ($\Delta G \approx -11.5\,\text{kcal} \cdot \text{mol}^{-1}$) was observed for PNSC123 (in which we studied two variants), although the interactions of this compound occur in the proximity of the N-terminal or C-terminus region, for each binding mode (in the upper right part of Figure 7D–F).

3.5 | ADMET Analysis

All evaluated compounds showed favorable intestinal permeability profiles, with most exhibiting excellent predicted Caco-2 permeability. However, differences were observed in human intestinal absorption (HIA), where CHEMBL3894860-variant2–variant4 showed poor or medium absorption, in contrast to CHEMBL2103870-variant4 and CHEMBL461101 variants, which displayed excellent absorption. Regarding P-glycoprotein (Pgp) interaction, all compounds were predicted as Pgp inhibitors, while only CHEMBL3894860 variants were identified as potential Pgp substrates (poor). In terms of distribution, all candidates demonstrated acceptable blood– brain barrier permeability (BBB) and high plasma protein binding (PPB). The metabolic profile revealed that most compounds were non-inhibitors and non-substrates of key cytochrome P450 isoenzymes (CYP1A2, CYP2C9, CYP2D6, CYP3A4), suggesting low metabolic interference. Finally, the toxicity assessment indicated noncarcinogenic and non-mutagenic (Ames test negative) properties for

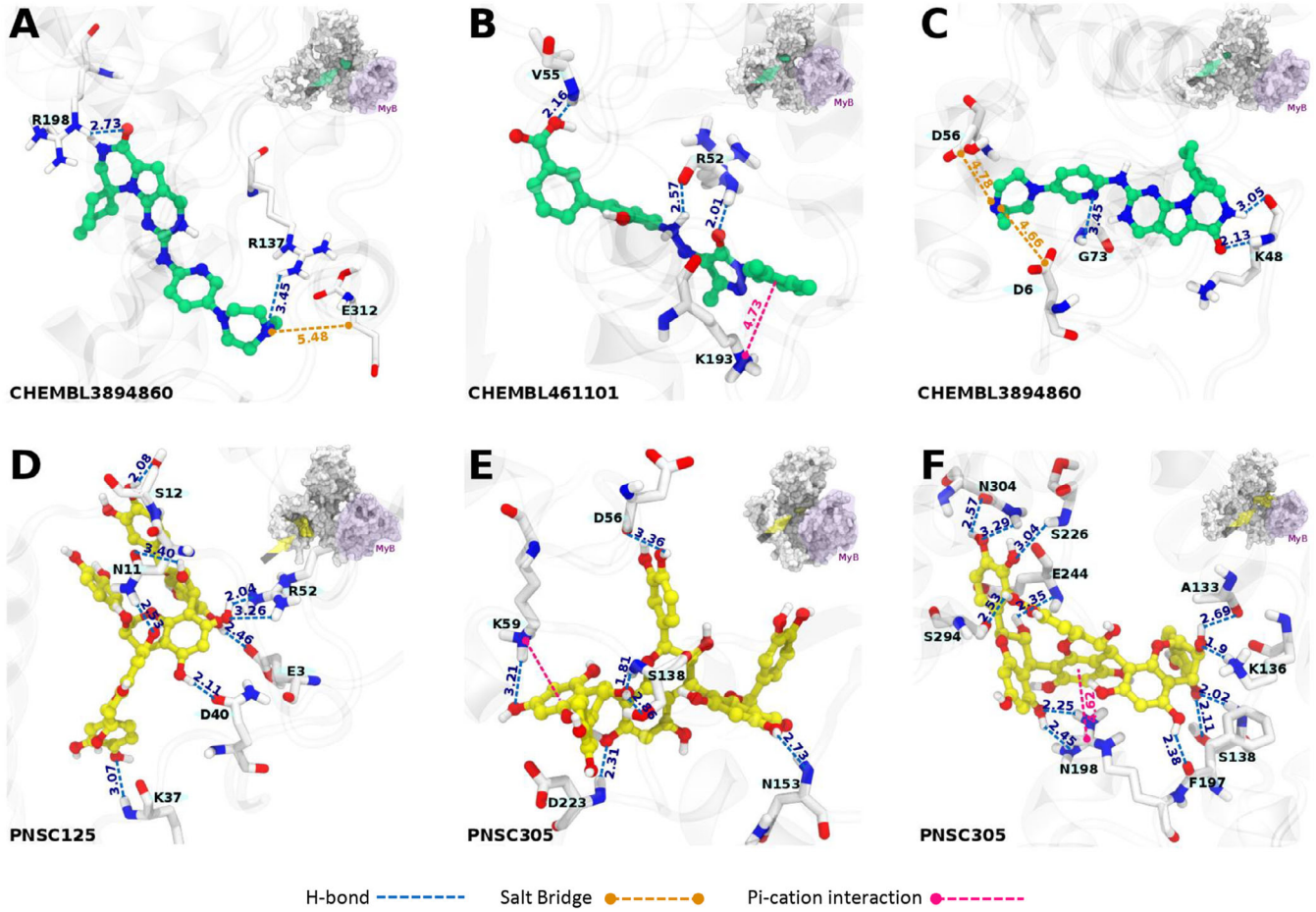

FIGURE 7 | 3D pose drug screened by docking in the telomere-binding protein model. Protein–ligand interactions are shown, with FDA-approved ligands in green and phytochemicals in yellow. At the upper right of each figure, are the sites where interactions occur. FDA, Food and Drug Administration.

all molecules, with no significant hERG inhibition predicted (Table 3).

4 | Discussion

The discovery of new inhibitory mechanisms for viruses is an area of study that is being supported by computational modeling tools [87]. Indeed, the availability of large amounts of omics information regarding organisms of interest, such as MPXV, supports the accelerated search for new pharmacological targets. Currently, drug targets (protein targets) can be classified into two classes: known drug targets and novel drug targets. For known drug targets, there is robust scientific evidence and available inhibitors; however, new drug targets also deserve attention as they may lead to new therapies [88].

Among the targets reported for MPXV, we know the F13 protein [89], vCCI protein [90], and H1 phosphatase [91]. A computational study also reported A48R (a thymidylate kinase), A50R (a DNA ligase), D13L (a major capsid protein), and I7L core proteinase (a cysteine proteinase), as potential drug targets for MPXV [92]. There have been no previous reports of using MPXV TBP in drug discovery. However, the study of telomeres and their accessory proteins has been previously described as an alternative in cancer treatment, mainly under two scopes: 1) inhibition of the telomerase enzyme or 2) destabilizing the structure of the telomere [93]. In our work, we propose targeting TBP-MPXV in a way to prevent virus maturation through destabilization of the protein-DNA interaction by a drug-mediated steric effect, since the absence of TBPs has been found to limit virion release in vaccinia virus recombinant assays [49]. Thus, our line of argument is that, similar to the absence of TBP, inhibition of TBP leads to suppression of the virus.

To model TBP-MPXV with high reliability, AlphaFold v2 software [68] is the best available method. It is well known that this algorithm correctly matches primary sequences with solved structures (templates); moreover, to date, a structural database with enough single domains has been claimed and thus AlphaFold solves the traditional problem of finding sequence-based templates with high accuracy, regardless of the evolutionary distance of proteins [94]. This allowed us to present a model with high accuracy when evaluating the pLDDT values, in which we achieved a sufficiently high degree of reliability for at least 83% of the amino acids (259/312 aa). It is worth mentioning that we have not found a similar structure available for TBP-MPXV, nor a complete sequence related protein solved, and for the TBPs found (1H6P, 5XYF, 1H6O, 2I0Q, and 3BUA) in the Protein Data Bank [95] the sequences, and therefore the

TABLE 1 | FDA-approved compounds.

Cut-off (nm)	Ensemble	Ligand	ΔG(kcal · mol^{-1})	K_d (nM)	$\bar{B}$	H-bonds		Hydrophobic Interactions		Other Interactions	
						N	residues	N	Residues	Type	Residue
0.3	E2	CHEMBL3894860-variant2	−10.1	37.12	0.242	2	R137, R198	4	A133, R134, F197, I307	SB	E312
0.2	E1	CHEMBL461101-variant1	−10.3	26.45	0.221	3	R52, R52, V55	5	V51, R52, P54, P54, K193	piCI	K193
0.3	E2	CHEMBL3894860-variant3	−10.2	31.34	0.21	3	K48, K48, G73	3	V51, P54, T194	SB	D6, D56
0.3	E2	CHEMBL3894860-variant5	−10.2	31.34	0.205	5	D6, K48, R52, R52, G73	6	V51, R52, P54, P54, D190, T194	SB	D56
										piCI	R52
0.5	E2	CHEMBL2103870-variant4	−10.1	37.12	0.185	4	A133, R134, S138, K221	4	R198, V219, R222, D223	SB	R198
										piS	F197
										HB	S225
0.2	E2	CHEMBL461101-variant3	−10.3	26.45	0.184	5	E224, S226, T301, V302, N304	7	V107, V107, I230, E298, E298, P303, N304	—	—
0.3	E2	CHEMBL461101-variant3	−10.3	26.45	0.184	4	A133, A133, R137, R137	7	R134, R137, F197, R198, V219, I307, E312	SB	K136, R198
										piS	F197
										piCI	R137
0.3	E2	CHEMBL461101-variant5	−10.2	31.34	0.177	5	R137, R137, S138, S138, D223	4	V103, R134, R137, F197	SB	R222
										piS	F197
										piCI	R137
0.3	E2	CHEMBL3894860-variant4	−10	43.98	0.176	5	A133, R137, S138, R198, S225	1	R134	—	—
0.4	E5	CHEMBL3894860-variant5	−10.1	37.12	0.173	4	S138, V219, V219, R222	1	V219	SB	E152

Note: Ligand interactions in the telomere-binding protein in the monkeypox virus model, interactions are ordered by the binding probability ($\bar{B}$) calculated by the Boltzmann equation.

TABLE 2 | Phytochemical compound interactions in the telomere-binding protein in the monkeypox virus model, interactions are ordered by the binding probability ($\bar{B}$) calculated by the Boltzmann equation.

Cut-off (nm)	Ensemble	Ligand	ΔG (kcal · mol^{-1})	K_d (nM)	$\bar{B}$	H-Bonds		Hydrophobic Interactions		Other Interactions	
						N	Residues	N	Residues	Type	Residue
0.2	E4	PNSC125-variant5	−12.6	0.53	0.619	9	E3, N11, N11, S12, K37, Q40, R52, R52, R52	9	I13, Y21, Y21, Y21, Y21, F22, P39, L78, L78	—	—
0.4	E4	PNSC305-variant3	−12.0	1.48	0.321	7	D56, K59, S138, S138, S138, N153, D223	4	R137, R137, T140, E152	piCI	K59
0.5	E1	PNSC305-variant1	−11.6	2.92	0.256	14	A133, K136, S138, S138, S138, F197, R198, R198, R198, E224, S226, S294, N304, N304	3	F197, D223, E224	piCI	R198
0.4	E4	PNSC305-variant5	−12	1.48	0.237	8	N80, K136, F197, R198, K221, K221, D223, S226	6	I76, I76, K129, V130, R218, K221	piCI	R198
0.2	E3	PNSC123-variant1	−11.5	3.46	0.229	6	V9, L18, K19, Y21, Y21, Q40	5	L8, V9, V9, L18, F22	—	—

(Continues)

TABLE 2 | (Continued)

Cut-off (nm)	Ensemble	Ligand	ΔG (kcal · mol^{-1})	K_d (nM)	$\bar{B}$	H-Bonds N	H-Bonds Residues	Hydrophobic Interactions N	Hydrophobic Interactions Residues	Other Interactions Type	Other Interactions Residue
0.5	E4	PNSC125-variant4	−11.2	5.76	0.189	13	D6, Q7, Q7, S12, S12, R52, V55, N143, N145, G146, R195, R195, R195	6	F4, D6, Q7, V9, R52, T194	—	—
0.2	E1	PNSC305-variant1	−11.4	4.1	0.182	15	A133, K136, S138, S138, S138, F197, R198, R198, R198, R218, K221, S294, S294, V302, N304	4	F197, R198, D223, V297	piCI	R198
0.3	E1	PNSC305-variant1	−11.4	4.1	0.182	15	K136, S138, S138, S138, F197, R198, R198, R198, R218, K221, E224, S294, S294, V302, N304	4	F197, R198, D223, V297	piCI	R198
0.5	E1	PNSC123-variant2	− 11.2	5.76	0.176	10	S138, S138, L196, R198, R218, D223, S225, S226, N304, I305	3	T105, R137, F197	—	—
0.5	E1	PNSC305-variant5	−11.8	2.08	0.169	8	A133, F197, R198, R198, R198, E224, S294, N304	3	R134, F197, E224	piCI	R198

TABLE 3 | ADMET analysis of the main FDA and phytochemical compounds for TBP inhibition.

Class	Properties	CHEMBL2103870-v4	CH3894860-v2	CH3894860-v3	CH3894860-v4	CH3894860-v5a	CH3894860-v5b	CH461101-v1	CH461101-v3a	CH461101-v3b	CH461101-v5
Absorption	Caco-2	Excellent	Excellent	Excellent	Excellent	Excellent	Excellent	Excellent	Excellent	Excellent	Excellent
	HIA	Excellent	Poor	Poor	Poor	Medium	Medium	Excellent	Excellent	Excellent	Excellent
	Pgp inhibitor	Excellent	Excellent	Excellent	Excellent	Excellent	Excellent	Excellent	Excellent	Excellent	Excellent
	Pgp substrate	Excellent	Poor	Poor	Poor	Poor	Poor	Excellent	Excellent	Excellent	Excellent
Distribution	BBB	Poor	Poor	Poor	Poor	Poor	Poor	Poor	Poor	Poor	Poor
	PPB	Poor	Poor	Excellent	Excellent	Excellent	Excellent	Excellent	Excellent	Excellent	Excellent
	Fu	Excellent	Excellent	Excellent	Excellent	Excellent	Excellent	Excellent	Excellent	Excellent	Excellent
Toxicity	Acute	Poor	Poor	Poor	Poor	Poor	Poor	Poor	Poor	Poor	Poor
	hERG	Excellent	Excellent	Excellent	Excellent	Excellent	Excellent	Excellent	Excellent	Excellent	Excellent
	Human	Poor	Poor	Poor	Poor	Poor	Poor	Poor	Poor	Poor	Poor
	Ames	Excellent	Excellent	Excellent	Excellent	Excellent	Excellent	Excellent	Excellent	Excellent	Excellent
	Carcinogenicity	Excellent	Excellent	Excellent	Excellent	Excellent	Excellent	Excellent	Excellent	Excellent	Excellent
Metabolism	CYP1A2 inhibition	No	No	No	No	No	No	No	No	No	No

(Continues)

TABLE 3 | (Continued)

Class	Properties	CHEMBL2103870-v4	CH3894860-v2	CH3894860-v3	CH3894860-v4	CH3894860-v5a	CH3894860-v5b	CH461101-v1	CH461101-v3a	CH461101-v3b	CH461101-v5
CYP1A2 substrate	No	No	No	No	No	No	No	No	No	No	
CYP2C19 inhibition	No	No	No	No	No	No	No	No	No	No	
CYP2C19 substrate	Yes	Yes	Yes	Yes	Yes	Yes	Yes	Yes	Yes	Yes	
CYP2C9 inhibition	Medium	Medium	No	No	No	No	No	No	No	No	
CYP2C9 substrate	Yes	Yes	Yes	Yes	Yes	Yes	Yes	Yes	Yes	Yes	
CYP2D6 inhibition	No	No	No	No	No	No	No	No	No	No	
CYP2D6 substrate	Medium	Medium	No	No	No	No	No	No	No	No	
	CYP3A4 inhibition	Medium	Medium	No	No	No	No	No	No	No	No
	CYP3A4 substrate	Yes	Yes	Yes	Yes	Yes	Yes	Yes	Yes	Yes	Yes

Abbreviations: FDA, Food and Drug Administration; TBP, telomere-binding protein.

structures, are markedly different. In that sense, this protein could not be modeled by other methods, as we have observed in another study that modeled all MPXV proteins by homology [96]. Surprisingly, in a study that addressed MPXV proteome modeling, the same methodology used in this research was used to solve the structure of TBP-MPX, with which, compared to our model, we obtained an almost identical structure (RMSD = 0.0866 Å) [97], which supports the model presented here.

When analyzing structural changes throughout molecular dynamics, we observe a structural similarity to DNA or RNA polymerase structures, in which, in our view, the motif Myb (229V-301T) would be similar to a thumb domain; the upper domain (142F-219V) would form a finger domain; and the central region (51V-140T), or the core, would be equivalent to a palm domain [98–100]. In particular, the perceived finger domain and thumb domain acquire flexibility by two characteristic loops near the central region (L135-Q141 and T220-Y228). We consider highly relevant the position of this pair of loops, since they confer a wide flexibility between domains, suggesting that this could be a mechanism by which the binding to the telomeric region occurs. On the other hand, the N-terminal domain, which in our simulation is exceptionally flexible, has been reported to be involved in the formation and stabilization of the telomere structure, due to its ability to mediate strand invasion that results in the formation of t-loops and to bind DNA junctions [42]. Furthermore, we remark that all these regions together cause the formation of a tunnel-like space, which would support DNA binding: this space can also be used for drug targeting.

To explore the pharmacological capacity of TBP-MPX, we employed a docking ensemble methodology with which we significantly expanded the search in conformational space. Currently, there is no standard methodology to correctly predict drug binding [101]. Since proteins are dynamic structures, the ensemble docking approach helps to explore transitions between different states in which a compound can bind [102]. In our study, we confirmed this principle by finding statistical differences between the evaluated ensembles. We also increased the robustness of the search by exploring different structural variants that our ligands could present, such as different ionizations, tautomerisms and variations in ring conformation. This has led us to observe that a ligand can acquire different conformations and, more importantly, different protonation states; this implies searching for the same molecule with a different number and position of hydrogen atoms. Since molecules can be found in different states, both chemical and energetic, depending on physiological or experimental conditions, this channeling makes our approach more reliable.

In ensemble-guided molecular docking, distinguishing between true binding modes and docking artifacts critically depends on the statistical and structural analysis of docking results across multiple protein conformations. Applying RMSD cutoffs (e.g., 0.2–0.5 nm) allows for classification of poses based on their geometric similarity to a reference or among a group of poses, with lower RMSD values, typically indicating greater structural consistency and, by extension, increased likelihood of representing a physically meaningful binding mode. The use of the Kruskal–Wallis test provides a non-parametric method for detecting statistically significant differences across multiple docking ensembles or conditions, ensuring that observed clustering of high-quality binding poses is not due to random chance. Following this, the Holm–Bonferroni post hoc procedure systematically controls for Type-I errors when conducting multiple comparisons, reducing the likelihood of false positives when identifying sets of poses or conditions that genuinely stand out across the ensemble. A true binding mode is expected to be reproducible in several ensemble members, yielding consistently low RMSD from the best-scoring or experimentally validated reference pose. In contrast, fake docking artifacts often manifest sporadic, outlier configurations that fail to achieve statistical significance when tested against the overall distribution of results. Ensemble docking approaches specifically address the limitations of single structure docking by incorporating protein flexibility, where genuine binding modes should demonstrate stability across multiple conformations while artifacts typically appear inconsistently. By applying rigorous statistical thresholds and post hoc corrections after RMSD-based clustering, only those pose groups surviving multiple hypothesis testing can be considered putative true binding modes, while others are more likely spurious docking artifacts. This integrated approach, as supported in the literature, enhances the reliability of docking predictions by leveraging both structural convergence and statistical rigor to separate signal from noise in complex ensemble docking workflows [103–109].

Reportedly, the Myb motif is important for DNA binding. Therefore, we focus on targeting those residues, which are important for DNA binding. Here, in TRF1 and TRF2 there is a highly conserved motif, KDXXR, which is remarkably important for specific binding of T [A/T] to GGG [110]. In TBP-MPXV, this motif is not conserved and is replaced by $_2$96VVECL$_3$01, however, it is followed by a residue, T301, that is highly conserved compared to TRF1 and TRF2. Additionally, we note that out of all our hits, PNSC305 interacts with a residue of this motif (V297) and CHEMBL461101 is the one that presented the most interactions close to this motif (E298 and T301). Likewise, we emphasize the occupancy of these ligands within the site that would serve for DNA binding, leaving the evaluation of the stability of these ligands in the corresponding sites to support the drugability of this protein.

Despite the promising selectivity profile of viral TBP inhibitors, potential risks at the host–pathogen interface warrant careful consideration to ensure therapeutic safety. While viral TBP Myb-domains share minimal sequence identity (15%–18%) with human Myb-family proteins and display divergent helix orientations and surface charges that reduce direct inhibition risks, the complex nature of viral–host interactions introduces additional considerations [47]. The distinct DNA-binding specificities provide another layer of selectivity, as viral TBP recognizes unique hairpin telomere structures absent in human chromosomal DNA, contrasting with human Myb proteins that bind linear consensus motifs (YAACNG) [47, 52]. However, the presence of host factors such as La-related protein 4 that colocalize with viral factories and interact indirectly with viral TBP raises theoretical concerns about potential disruption of host–virus interactions that may be critical for mounting effective innate immune responses, though current evidence indicates no direct binding interface overlap with the targeted compound sites [111].

In addition to the selectivity considerations discussed above, it is also important to consider the broader pharmacokinetic performance of the potential inhibitor. While our selected phytochemical candidates demonstrated promising pharmacokinetic and safety profiles (e.g., good HIA, Caco-2 permeability, low Pgp substrate risk), it is important to compare these outcomes against the top FDA compounds. On one hand, the fact that phytochemicals originate from nature and often carry multifaceted bioactivities is a clear strength, as recent reviews highlight, the chemical diversity of plant-derived metabolites offers a rich reservoir for novel therapeutic leads [112]. On the other hand, FDA-approved drugs typically undergo rigorous optimization for drug-likeness (e.g., Lipinski rule), manufacturability and reproducible ADMET profiles (as determined for most of the classes in Table S4), while many phytochemical may not yet fully satisfy all. For example, although some natural compounds can match or even exceed binding affinities seen in approved drugs, they often have challenges like high polarity, low oral bioavailability, or unpredictable metabolism. In our data, the phytochemical variants that achieved excellent absorption and non-inhibitor metabolism status may therefore represent strong starting points for drug development (scaffolds), but they still require a degree of optimization and further studies. Furthermore, whereas approved drugs often carry extensive in vivo and clinical data, phytochemicals remain underexplored. To date, only a small fraction of the phytochemical space has been screened for biological activity or progressed toward approval. In that sense, further study of the pharmacodynamics of top phytochemicals is required.

Additionally, our sequence alignment between MPXV-TBP and the human homologs TERF1 and TERF2 (UniProt IDs: P54274 and Q15554) shows a clear divergence at the residues forming the ligand-binding pockets (Pockets 1 and 2 in Figure S3). In MPXV-TBP these pockets are composed of positively charged or hydrophobic residues, while the corresponding positions in human TERFs contain polar or negatively charged substitutions with different spatial orientations. For example, regions around residues 125–140 and 210–240 show no conservation and would not reproduce the electrostatic or steric environment of the viral pockets. These differences in charge, size, and aromaticity support a high degree of selectivity for our hits, reducing the likelihood of off-target interactions with human TBPs.

To address these potential risks, a comprehensive mitigation strategy incorporating both computational and experimental approaches is essential for developing safe TBP-targeted therapeutics. Structure-guided optimization offers a pathway to enhance selectivity by exploiting viral-specific pocket residues such as V296 and E300 that are absent in human TBPs, allowing for the rational design of inhibitors with minimal host protein interaction [47]. Empirical validation through cytotoxicity screening in human cell lines remains crucial to rule out unintended modulation of host TBP function or disruption of essential cellular processes. While the structural divergence and unique telomere recognition mechanisms of viral TBP support a favorable risk-benefit profile compared to current therapeutics with known toxicities, rigorous off-target screening and careful monitoring of host–pathogen interface effects will be essential to ensure that TBP inhibition provides therapeutic benefit without compromising host cellular functions or immune responses. This balanced approach acknowledges both the promising selectivity features and the need for thorough safety evaluation in the development of these novel antiviral agents.

While this study represents a computational investigation, we fully recognize the critical importance of experimental validation to confirm our theoretical predictions. To bridge this gap between in silico findings and practical application, some experimental approaches can be taken. The recombinant expression and purification of His-tagged MPXV TBP, verified through circular dichroism spectroscopy, provides a robust platform for high-throughput screening that surpasses the technical challenges associated with validating current drug targets [51]. The implementation of competitive DNA-binding assays using EMSAs with fluorescently labeled telomeric hairpin oligonucleotides offers precise quantification of inhibitor potency through IC_{50} determination, exemplified by compounds like PNSC125 [47]. This approach is complemented by isothermal titration calorimetry studies that provide comprehensive thermodynamic profiles (ΔG, ΔH, and stoichiometry), building upon established VACV TBP-ligand methodologies to ensure thorough characterization of drug-target interactions [52]. The translational relevance of TBP targeting is further strengthened by the integration of viral growth inhibition assays in MPXV-infected cell cultures, utilizing both plaque-reduction and qPCR-based viral load measurements to determine EC_{50} values according to established orthopoxvirus protocols [113]. Critically, the mutational validation strategy employing specific TBP variants (R137A, R198A) provides definitive proof of target engagement by comparing compound efficacy against wild-type protein in both DNA-binding and viral assays [51]. This comprehensive experimental framework not only validates computational predictions but also establishes a clear path for developing TBP inhibitors with demonstrable biochemical specificity and antiviral efficacy-advantages that current therapeutics have struggled to achieve due to resistance emergence, toxicity concerns, and limited mechanistic diversity.

5 | Conclusion

Using computational tools, we have proposed a highly reliable model of TBP-MPX and described basic structural information about its major domains. Furthermore, we propose this poorly studied protein as a new drug target for the treatment of monkeypox disease. Our ensemble docking approach demonstrates that it is possible to improve conformational sampling to achieve better prediction of binding mode and binding energy; thus, loss of information is avoided. Furthermore, it has been observed that TBP-MPX is able to bind drugs with binding energies higher than 10 kcal mol^{-1}, suggesting a high affinity of this protein to bind favorably to inhibitors. In this context, we determined that three FDA-approved compounds, CHEMBL3894860, CHEMBL461101, and CHEMBL2103870, and three phytocompounds, PNSC125, PNSC123, and PNSC305, showed the best interaction energies after a comprehensive search. These compounds can be evaluated in further experimental assays or used as lead compounds in pharmacophore models.

Acknowledgments

We express our gratitude to the administrators of MANATI supercomputer, where virtual screening assays were performed, in the facilities of the Centro de Alto Rendimiento Computacional de la Amazonía Peruana - Instituto de Investigaciones de la Amazonía Peruana. More information can be found at: http://www.iiap.gob.pe/web/manati.aspx/. I. C. is grateful to the Brazilian funding agency CNPq for the research scholarship (304937/2023-1). This study was financed in part by the Coordenação de Aperfeiçoamento de Pessoal de Nível Superior-Brasil (CAPES)-Finance code 001. Part of the computational results presented here were developed with the help of CENAPAD-SP (Centro Nacional de Processamento de Alto Desempenho em São Paulo) grant UNICAMP/FINEP-MCT, the National Laboratory for Scientific Computing (LNCC/MCTI, Brazil) for providing HPC resources of the Santos Dumont supercomputer, and CENAPAD-UFC (Centro Nacional de Processamento de Alto Desempenho, at Universidade Federal do Ceará).

The Article Processing Charge for the publication of this research was funded by the Coordenação de Aperfeiçoamento de Pessoal de Nível Superior - Brasil (CAPES) (ROR identifier: 00x0ma614).

Author Contributions

Edinson Gervacio-Villarreal: formal analysis, writing – original draft preparation, writing – reviewing and editing. **Georcki Ropön-Palacios**: conceptualization, methodology, software, investigation, formal analysis, validation, writing – original draft preparation, writing – reviewing and editing. **Claudina Sancho**: data curation, writing – reviewing and editing. **Jhon Pérez-Silva**: methodology, software. **Kewin Otazu**: visualization, formal analysis. **Gustavo E. Olivos-Ramirez**: visualization, formal analysis. **Karolyn Vega-Chozo**: visualization, formal analysis. **Yaritza L. Ramirez-Díaz**: data curation, software. **Manuel E. Chenet-Zuta**: reviewing and editing. **Ivonne Navarro del Aguila**: reviewing and editing. **Mario De la Cruz Flores**: reviewing and editing. **Cinthia Aguiar**: writing – original draft preparation, writing – reviewing and editing. **Ihosvany Camps**: conceptualization, supervision, running computations, writing – reviewing and editing.

Conflicts of Interest

The authors declare that they have no known competing financial interests or personal relationships that could appear to influence the work reported in this article.

Data Availability Statement

The raw data required to reproduce these findings are available to download from Zenodo repository, https://doi.org/10.5281/zenodo.17858037.

References

1. O. Uwishema, O. Adekunbi, C. A. Peñamante, et al., "The Burden of Monkeypox Virus Amidst the Covid-19 Pandemic in Africa: A Double Battle for Africa," *Annals of Medicine and Surgery* 80 (2022): 104197.

2. N. G. Naga, E. A. Nawar, A. A. Mobarak, A. G. Faramawy, and H. M. H. Al-Kordy, "Monkeypox: A Re-Emergent Virus With Global Health Implications – A Comprehensive Review," *Tropical Diseases, Travel Medicine and Vaccines* 11 (2025): 2.

3. World Health Organization, "Multi-Country Outbreak of Mpox External Situation Report 31," https://www.who.int/emergencies/disease-outbreak-news/item/2023-DON493, 2023, Accessed: 2024-03-22.

4. D. G. Diven, "An Overview of Poxviruses," *Journal of the American Academy of Dermatology* 44 (2001): 1–16.

5. J. G. Fox, G. Otto, and L. A. Colby, "Chapter 28 - Selected Zoonoses," in *Laboratory Animal Medicine (Third Edition)*, third edition ed., ser. American College of Laboratory Animal Medicine, ed. J. G. Fox, L. C. Anderson, G. M. Otto, K. R. Pritchett-Corning, and M. T. Whary (Academic Press, 2015), 1313–1370, https://www.sciencedirect.com/science/article/pii/B9780124095274000286.

6. L. Khodakevich, Z. Ježek, and D. Messinger, "Monkeypox Virus: Ecology and Public Health Significance," *Bulletin of the World Health Organization* 66 (1988): 747.

7. S. Rampogu, Y. Kim, S.-W. Kim, and K. W. Lee, "An Overview on Monkeypox Virus: Pathogenesis, Transmission, Host Interaction and Therapeutics," *Frontiers in Cellular and Infection Microbiology* 13 (2023): 1076251.

8. C. Suñer, M. Ubals, E. J. Tarín-Vicente, et al., "Viral Dynamics in Patients With Monkeypox Infection: A Prospective Cohort Study in Spain," *Lancet Infectious Diseases* 23 (2023): 445–453.

9. P. Satapathy, S. Rustagi, A. Neyazi, et al., "First Human Death Due to Monkeypox Virus in Pakistan: A Public Health Concern for Resource-Limited Non-Endemic Countries," *International Journal of Surgery Global Health* 7 (2024): e0407.

10. C. T. Cho and H. A. Wenner, "Monkeypox Virus," *Bacteriological reviews* 37 (1973): 1–18.

11. Y. Sun, W. Nie, D. Tian, and Q. Ye, "Human Monkeypox Virus: Epidemiologic Review and Research Progress in Diagnosis and Treatment," *Journal of Clinical Virology Plus* 171 (2024): 105662.

12. S. N. Shchelkunov, A. V. Totmenin, I. V. Babkin, et al., "Human Monkeypox and Smallpox Viruses: Genomic Comparison," *FEBS Letters* 509 (2001): 66–70.

13. A. Fowotade, T. Fasuyi, and R. Bakare, "Re-Emergence of Monkeypox in Nigeria: A Cause for Concern and Public Enlightenment," *African Journal of Clinical and Experimental Microbiology* 19 (2018): 307.

14. K. Sagdat, A. Batyrkhan, and D. Kanayeva, "Exploring Monkeypox Virus Proteins and Rapid Detection Techniques," *Frontiers in Cellular and Infection Microbiology* 14 (2024): 1414224.

15. N. Girometti, R. Byrne, M. Bracchi, et al., "Demographic and Clinical Characteristics of Confirmed Human Monkeypox Virus Cases in Individuals Attending A Sexual Health Centre in London, UK: An Observational Analysis," *Lancet Infectious Diseases* 22 (2022): 1321–1328.

16. A. Antinori, V. Mazzotta, S. Vita, et al., "Epidemiological, Clinical and Virological Characteristics of Four Cases of Monkeypox Support Transmission Through Sexual Contact, Italy, May 2022," *Eurosurveillance* 27 (2022): 2200421.

17. M. M. Alshamrani, A. El-Saed, S. Al-Fayez, et al., "Routes of Transmission of Mpox by Virus Clade and Geographic Distribution: A Systematic Review," *Journal of Infection and Public Health* 18 (2025): 102985.

18. C. L. Hutson, D. S. Carroll, N. Gallardo-Romero, et al., "Monkeypox Disease Transmission in an Experimental Setting: Prairie Dog Animal Model," *PLos One* 6 (2011): 1–12.

19. A. Peiró-Mestres, I. Fuertes, D. Camprubí-Ferrer, et al., "Frequent Detection of Monkeypox Virus DNA in Saliva, Semen, and Other Clinical Samples From 12 Patients, Barcelona, Spain, May to June 2022," *Eurosurveillance* 27 (2022): 2200503.

20. N. Berthet, S. Descorps-Declère, C. Besombes, et al., "Genomic History of Human Monkey Pox Infections in the Central African Republic Between 2001 and 2018," *Scientific Reports* 11 (2021): 13085.

21. E. M. Bunge, B. Hoet, L. Chen, et al., "The Changing Epidemiology of Human Monkeypox—A Potential Threat? A Systematic Review," *PLOS Neglected Tropical Diseases* 16 (2022): 1–20.

22. J. Isidro, V. Borges, M. Pinto, et al., "Phylogenomic Characterization and Signs of microevolution in the 2022 Multi-Country Outbreak of Monkeypox Virus," *Nature Medicine* 28 (2022): 1569–1572.

23. L. Wang, J. Shang, S. Weng, et al., "Genomic Annotation and Molecular Evolution of Monkeypox Virus Outbreak in 2022," *Journal of Medical Virology* 95 (2022): e28036.

24. J. R. Otieno, C. Ruis, A. B. Onoja, et al., "Global Genomic Surveillance of Monkeypox Virus," *Nature Medicine* 31 (2024): 342–350.

25. N. Ndodo, J. Ashcroft, K. Lewandowski, et al., "Distinct Monkeypox Virus lineages Co-Circulating in Humans Before 2022," *Nature Medicine* 29 (2023): 2317–2324.

26. A. O'Toole, R. A. Neher, N. Ndodo, et al., "APOBEC3 Deaminase Editing in Mpox Virus as Evidence for Sustained Human Transmission Since at Least 2016," *Science* 382 (2023): 595–600.

27. A. Malla and F. M. Saleh, "The Resurgence of Monkeypox Virus: A Critical Global Health Challenge and the Need for Vigilant Intervention," *Frontiers in Public Health* 13 (2025): 1572100.

28. P. Fine, Z. Jezek, B. Grab, and H. Dixon, "The Transmission Potential of Monkeypox Virus in Human Populations," *International Journal of Epidemiology* 17 (1988): 643–650.

29. G. A. Poland, R. B. Kennedy, and P. K. Tosh, "Prevention of Monkeypox With Vaccines: A Rapid Review," *Lancet Infectious Diseases* 22 (2022): e349–e358.

30. J. Wu and X. Zhang, "Exploring Monkeypox Virus Antibody Levels: Insights From Human Immunological Research," *Virology Journal* 22 (2025): 175.

31. G. Andrei and R. Snoeck, "Cidofovir Activity Against Poxvirus Infections," *Viruses* 2 (2010): 2803–2830.

32. V. A. Olson, S. K. Smith, S. Foster, et al., "In Vitro Efficacy of Brincidofovir Against Variola Virus," *Antimicrobial Agents and Chemotherapy* 58 (2014): 5570–5571.

33. S. E. Altmann, A. L. Smith, J. Dyall, et al., "Inhibition of Cowpox Virus and Monkeypox Virus Infection by Mitoxantrone," *Antiviral Research* 93 (2012): 305–308.

34. G. Yang, D. C. Pevear, M. H. Davies, et al., "An Orally Bioavailable Antipoxvirus Compound (St-246) Inhibits Extracellular Virus Formation and Protects Mice From Lethal Orthopoxvirus Challenge," *Journal of Virology* 79 (2005): 13139–13149.

35. H. Adler, S. Gould, P. Hine, et al., "Clinical Features and Management of Human Monkeypox: A Retrospective Observational Study in the UK," *Lancet Infectious Diseases* 22 (2022): 1153–1162.

36. H. Y. I. Lam, J. S. Guan, and Y. Mu, "In Silico Repurposed Drugs Against Monkeypox Virus," *Molecules* 27 (2022): 5277.

37. J. M. Garrigues, P. Hemarajata, A. Karan, et al., "Identification of Tecovirimat Resistance-Associated Mutations in Human Monkeypox Virus - Los Angeles County," *Antimicrobial Agents and Chemotherapy* 67 (2023): e00568–23.

38. T. G. Smith, C. M. Gigante, N. T. Wynn, et al., "Tecovirimat Resistance in Mpox Patients, United States, 2022–2023," *Emerging Infectious Disease* 29 (2023): 2426–2432.

39. X. Li, Z. Pan, and L. Zhang, "Tecovirimat: A Journey From Discovery to Mechanistic Insights in Poxvirus Inhibition," *PLoS Pathogens* 21 (2025): e1013140.

40. R. Vernuccio, A. Martínez León, C. S. Poojari, et al., "Structural Insights Into Tecovirimat Antiviral Activity and Poxvirus Resistance," *Nature Microbiology* 10 (2025): 734–748.

41. Y. Xiang and R. K. Lane, "Vaccinia Virus (poxviridae)," in *Encyclopedia of Virology (Fourth Edition)*, fourth edition ed., D. H. Bamford and M. Zuckerman, Eds. (Academic Press, 2021), 854–859.

42. N. V. Ilicheva, O. I. Podgornaya, and A. P. Voronin, "Chapter Three - Telomere Repeat-Binding Factor 2 is Responsible for the Telomere Attachment to the Nuclear Membrane," in *Advances in Protein Chemistry and Structural Biology*, ser. Advances in Protein Chemistry and Structural Biology, ed. R. Donev (Academic Press, 2015), 101, 67–96.

43. M. Kuchar, "Plant Telomere–Binding Proteins," *Biologia Plantarum* 50 (2006): 1–7.

44. J. D. Watson, A. Gann, T. A. Baker, M. Levine, S. P. Bell, and R. Losick, *Biología Molecular del Gen*, seventh edition ed. (Editorial Médica Panamericana-Español, 2014).

45. E. Lansiaux, N. Jain, S. Laivacuma, and A. Reinis, "The Virology of Human Monkeypox Virus (HMPXV): A Brief Overview," *Virus Research* 322 (2022): 198932.

46. Z. Yang, S. E. Reynolds, C. A. Martens, D. P. Bruno, S. F. Porcella, and B. Moss, "Expression Profiling of the Intermediate and Late Stages of Poxvirus Replication," *Journal of Virology* 85 (2011): 9899–9908.

47. J. DeMasi, S. Du, D. Lennon, and P. Traktman, "Vaccinia Virus Telomeres: Interaction With the Viral I1, I6, and K4 Proteins," *Journal of Virology* 75 (2001): 10 090–10 105.

48. I. Cohen-Gihon, O. Israeli, O. Shifman, et al., "Identification and Whole-Genome Sequencing of a Monkeypox Virus Strain Isolated in Israel," *Microbiology Resource Announcements* 9 (2020): e01524–19.

49. N. Klemperer, J. Ward, E. Evans, and P. Traktman, "The Vaccinia Virus I1 Protein is Essential for the Assembly of Mature Virions," *Journal of Virology* 71 (1997): 9285–9294.

50. E. B. Alencar Filho, R. F. Oliveira Neto, V. C. Santos, and A. L. S. Ferreira, "Deep Reinforcement Learning and Structure-Based Approaches in the De Novo Design of a New Potential Inhibitor of F13 Protein From Monkeypox Virus," *Journal of the Brazilian Chemical Society* 36 (2025): e-20250022.

51. O. Grubisha and P. Traktman, "Genetic Analysis of the Vaccinia Virus I6 Telomere-Binding Protein Uncovers a Key Role in Genome Encapsidation," *Journal of Virology* 77 (2003): 10 929–10 942.

52. M. M. Shenouda, R. S. Noyce, S. Z. Lee, et al., "The Mismatched Nucleotides Encoded in Vaccinia Virus Flip-and-Flop Hairpin Telomeres Serve an Essential Role in Virion Maturation," *PLoS Pathogens* 18 (2022): e1010392.

53. A. D. Prasetyo, H. Hudari, M. Permata, and N. A. Salin, "The Role of Tecovirimat in the Management of Monkeypox," *Bioscientia Medicina: Journal of Biomedicine and Translational Research* 8 (2024): 4600–4605.

54. H. Rafiq, J. Hu, M. A. Hakami, et al., "Identification of Novel STAT3 Inhibitors for Liver Fibrosis, Using Pharmacophore-Based Virtual Screening, Molecular Docking, and Biomolecular Dynamics Simulations," *Scientific Reports* 13 (2023): 20147.

55. A. Gaulton, A. Hersey, M. Nowotka, et al., "The ChEMBL Database in 2017," *Nucleic Acids Research* 45 (2016): D945–D954.

56. P. J. Ropp, J. O. Spiegel, J. L. Walker, et al., "Gypsum-DL: An Open-Source Program for Preparing Small-Molecule Libraries for Structure-Based Virtual Screening," *Journal of Cheminformatics* 11 (2019): 34, https://doi.org/10.1186/s13321-019-0358-3.

57. P. J. Ropp, J. C. Kaminsky, S. Yablonski, and J. D. Durrant, "Dimorphite-DL: An Open-Source Program for Enumerating the Ionization States of Drug-Like Small Molecules," *Journal of Cheminformatics* 11 (2019): 14.

58. G. M. Morris, R. Huey, W. Lindstrom, et al., "AutoDock4 and AutoDockTools4: Automated Docking With Selective Receptor Flexibility," *Journal of Computational Chemistry* 30 (2009): 2785–2791.

59. J. C. Aponte, A. J. Vaisberg, R. Rojas, et al., "A Multipronged Approach to the Study of Peruvian Ethnomedicinal Plants: A Legacy of the ICBG-Peru Project," *Journal of Natural Products* 72 (2009): 524–526.

60. M. Villena-Tejada, I. Vera-Ferchau, A. Cardona-Rivero, et al., "Use of Medicinal Plants for COVID-19 Prevention and Respiratory Symptom Treatment During the Pandemic in Cusco, Peru: A Cross-Sectional Survey," *PLOS ONE* 16 (2021): e0257165.

61. J. Horackova, M. E. Chuspe Zans, L. Kokoska, et al., "Ethnobotanical Inventory of Medicinal Plants Used by Cashinahua (Huni Kuin) Herbalists in Purus Province, Peruvian Amazon," *Journal of Ethnobiology and Ethnomedicine* 19 (2023): 16.

62. V. Roumy, A.-L. Gutierrez-Choquevilca, J. Lopez Mesia, et al., "In Vitro Antimicrobial Activity of Traditional Plant Used in Mestizo Shamanism From the Peruvian Amazon in Case of Infectious Diseases," *Pharmacognosy Magazine* 11 (2015): 625.

63. A. F. Yepes-Pérez, O. Herrera-Calderon, and J. Quintero-Saumeth, "Uncaria Tomentosa(Cat's Claw): A Promising Herbal Medicine Against SARS-CoV-2/ACE-2 Junction and SARS-CoV-2 Spike Protein Based on Molecular Modeling," *Journal of Biomolecular Structure and Dynamics* 40 (2020): 2227–2243.

64. A. F. Yepes-Pérez, O. Herrera-Calderón, C. A. Oliveros, et al., "The Hydroalcoholic Extract of *Uncaria tomentosa* (Cat's Claw) Inhibits the Infection of Severe Acute Respiratory Syndrome Coronavirus 2 (SARS-CoV-2) *In Vitro*," *Evidence-Based Complementary and Alternative Medicine* 2021 (2021): 1–11.

65. L. D. Goyzueta-Mamani, H. L. Barazorda-Ccahuana, K. Mena-Ulecia, and M. A. Chávez-Fumagalli, "Antiviral Activity of Metabolites From Peruvian Plants Against SARS-CoV-2: An In Silico Approach," *Molecules* 26 (2021): 3882.

66. E. M. C. Peñaloza, S. S. Costa, and O. Herrera-Calderon, "Medicinal Plants in Peru as a Source of Immunomodulatory Drugs Potentially Useful Against COVID-19," *Revista Brasileira de Farmacognosia* 33 (2023): 237–258.

67. The UniProt Consortium, A. Bateman, M.-J. Martin, S. Orchard, et al., "UniProt: The Universal Protein Knowledgebase in 2021," *Nucleic Acids Research* 49 (2021): D480–D489.

68. J. Jumper, R. Evans, A. Pritzel, et al., "Highly Accurate Protein Structure Prediction With AlphaFold," *Nature* 596 (2021): 583–589.

69. U. Bodenhofer, E. Bonatesta, C. Horejš-Kainrath, and S. Hochreiter, "MSA: An R Package for Multiple Sequence Alignment," *Bioinformatics* 31 (2015): 3997–3999.

70. R Core Team, R Foundation for Statistical Computing, Vienna, Austria, 2021. [Online]. Available: https://cran.r-project.org/doc/FAQ/R-FAQ.html#Citing-R.

71. E. Jurrus, D. Engel, K. Star, et al., "Improvements to the APBS Biomolecular Solvation Software Suite," *Protein Science* 27 (2018): 112–128.

72. S. Jo, T. Kim, V. G. Iyer, and W. Im, "CHARMM-GUI: A Web-Based Graphical User Interface for CHARMM," *Journal of Computational Chemistry* 29 (2008): 1859–1865.

73. W. Jorgensen, J. Chandrasekhar, J. Madura, R. Impey, and M. Klein, "Comparison of Simple Potential Functions for Simulating Liquid Water," *Journal of Chemical Physics* 79 (1983): 926–935, https://doi.org/10.1063/1.445869.

74. M. J. Abraham, T. Murtola, R. Schulz, et al., "GROMACS: High Performance Molecular Simulations Through Multi-Level Parallelism From Laptops to Supercomputers," *SoftwareX* 1-2 (2015): 19–25.

75. M. Meyer and V. Pontikis, Eds., *Computer Simulation in Materials Science* (Springer Netherlands, 1991).

76. M. Parrinello and A. Rahman, "Polymorphic Transitions in Single Crystals: A New Molecular Dynamics Method," *Journal of Applied Physics* 52 (1981): 7182–7190.

77. B. Hess, H. Bekker, H. J. C. Berendsen, and J. G. E. M. Fraaije, "Lincs: A Linear Constraint Solver for Molecular Simulations," *Journal of Computational Chemistry* 18 (1997): 1463–1472.

78. S. Miyamoto and P. A. Kollman, "Settle: An Analytical Version of the Shake and Rattle Algorithm for Rigid Water Models," *Journal of Computational Chemistry* 13 (1992): 952–962.

79. H. G. Petersen, "Accuracy and Efficiency of the Particle Mesh Ewald Method," *Journal of Chemical Physics* 103 (1995): 3668–3679.

80. X. Daura, K. Gademann, B. Jaun, D. Seebach, W. F. van Gunsteren, and A. E. Mark, "Peptide Folding: When Simulation Meets Experiment," *Angewandte Chemie International Edition* 38 (1999): 236–240.

81. O. Trott and A. J. Olson, "AutoDock Vina: Improving the Speed and Accuracy of Docking With a New Scoring Function, Efficient Optimization, and Multithreading," *Journal of Computational Chemistry* (2009): NA–NA.

82. K. E. Rogers, H. Keränen, J. D. Durrant, et al., "Novel Cruzain Inhibitors for the Treatment of Chagas' Disease," *Chemical Biology & Drug Design* 80 (2012): 398–405.

83. M. F. Adasme, K. L. Linnemann, S. N. Bolz, et al., "PLIP 2021: Expanding the Scope of the Protein-Ligand Interaction Profiler to DNA and RNA," *Nucleic Acids Research* 49 (2021): W530–W534, https://doi.org/10.1093/nar/gkab294.

84. I. Patil, "Visualizations With Statistical Details: The 'ggstatsplot' approach," *Journal of Open Source Software* 6 (2021): 3167.

85. H. Wickham, *ggplot2: Elegant Graphics for Data Analysis* (Springer-Verlag New York, 2016).

86. G. Xiong, Z. Wu, J. Yi, et al., "Admetlab 2.0: An Integrated Online Platform for Accurate and Comprehensive Predictions of Admet Properties," *Nucleic Acids Research* 49 (2021): W5–W14.

87. M. Schenone, V. Dancik, B. K. Wagner, and P. A. Clemons, "Target Identification and Mechanism of Action in Chemical Biology and Drug Discovery," *Nature Chemical Biology* 9 (2013): 232–240.

88. J. Paananen and V. Fortino, "An Omics Perspective on Drug Target Discovery Platforms," *Briefings in Bioinformatics* 21 (2020): 1937–1953.

89. D. Li, Y. Liu, K. Li, and L. Zhang, "Targeting F13 From Monkeypox Virus and Variola Virus by Tecovirimat: Molecular Simulation Analysis," *Journal of Infection* 85 (2022): e99–e101.

90. J. M. Jones, I. Messauodi, R. D. Estep, B. Orzechowska, and S. W. Wong, "Monkeypox Virus Viral Chemokine Inhibitor (MPV VCCI), a Potent Inhibitor of Rhesus Macrophage Inflammatory Protein-1," *Cytokine* 43 (2008): 220–228.

91. W. Cui, H. Huang, Y. Duan, et al., "Crystal Structure of Monkeypox H1 Phosphatase, an Antiviral Drug Target," Protein Cell 14 (2022): 469–472.

92. H. Y. I. Lam, J. S. Guan, and Y. Mu, "In Silico Repurposed Drugs Against Monkeypox Virus," *Molecules* 27 (2022): 5277.

93. J. Cookson and C. Laughton, "The Levels of Telomere-Binding Proteins in Human Tumours and Therapeutic Implications," *European Journal of Cancer* 45 (2009): 536–550.

94. J. Skolnick, M. Gao, H. Zhou, and S. Singh, "Alphafold 2: Why It Works and Its Implications for Understanding the Relationships of Protein Sequence, Structure, and Function," *Journal of Chemical Information and Modeling* 61 (2021): 4827–4831.

95. Y. Gao, L. Yan, Y. Huang, et al., "Structure of the RNA-Dependent RNA Polymerase From COVID-19 Virus," *Science* 368 (2020): 779–782.

96. L. Parigger, A. Krassnigg, S. Grabuschnig, et al., "AI-Assisted Structural Consensus-Proteome Prediction of Human Monkeypox Viruses Isolated Within a Year After the 2022 Multi-Country Outbreak," *Microbiology Spectrum* 11 (2022): e02 315–23.

97. L. Zheng, J. Meng, M. Lin, et al., "Structure Prediction of the Entire Proteome of Monkeypox Variants," *Acta Materia Medica* 1 (2022): 260–264.

98. R. G. Federley and L. J. Romano, "DNA Polymerase: Structural Homology, Conformational Dynamics, and the Effects of Carcinogenic DNA Adducts," *Journal of Nucleic Acids* 2010 (2010): 457176.

99. N. Yao and M. O'Donnell, "Comparison of Bacterial and Eukaryotic Replisome Components," in *Encyclopedia of Cell Biology*, ed. R. A. Bradshaw and P. D. Stahl (Academic Press, 2016), 396–417.

100. R. Jácome, A. Becerra, S. Ponce de León, and A. Lazcano, "Structural Analysis of Monomeric RNA-Dependent Polymerases: Evolutionary and Therapeutic Implications," *PloS one* 10 (2015): e0139001.

101. P. H. Torres, A. C. Sodero, P. Jofily, and F. P. Silva-Jr, "Key Topics in Molecular Docking for Drug Design," *International Journal of Molecular Sciences* 20 (2019): 4574.

102. K. Kapoor, S. Thangapandian, and E. Tajkhorshid, "Extended-Ensemble Docking to Probe Dynamic Variation of Ligand Binding Sites During Large-Scale Structural Changes of Proteins," *Chemical Science* 13 (2022): 4150–4169.

103. Y. Awuni and Y. Mu, "Reduction of False Positives in Structure-Based Virtual Screening when Receptor Plasticity is Considered," *Molecules* 20 (2015): 5152–5164.

104. R. De Paris, C. V. Quevedo, D. D. Ruiz, O. Norberto de Souza, and R. C. Barros, "Clustering Molecular Dynamics Trajectories for Optimizing Docking Experiments," *Computational Intelligence and Neuroscience* 2015 (2015): 916240.

105. S. Makeneni, D. F. Thieker, and R. J. Woods, "Applying Pose Clustering and MD Simulations to Eliminate False Positives in Molecular Docking," *Journal of Chemical Information and Modeling* 58 (2018): 605–614.

106. K. Palacio-Rodríguez, I. Lans, C. N. Cavasotto, and P. Cossio, "Exponential Consensus Ranking Improves the Outcome in Docking and Receptor Ensemble Docking," *Science Reports* 9 (2019): 5142.

107. S. Mohammadi, Z. Narimani, M. Ashouri, R. Firouzi, and M. H. Karimi-Jafari, "Ensemble Learning From Ensemble Docking: Revisiting the Optimum Ensemble Size Problem," *Science Reports* 12 (2022): 410.

108. J. L. Gan, D. Kumar, C. Chen, et al., "Benchmarking Ensemble Docking Methods in D3R Grand Challenge 4," *Journal of Computer-Aided Molecular Design* 36 (2022): 87–99.

109. K. McKay, N. B. Hamilton, J. M. Remington, S. T. Schneebeli, and J. Li, "Essential Dynamics Ensemble Docking for Structure-Based GPCR Drug Discovery," *Frontiers in Molecular Biosciences* 9 (2022): 879212.

110. M. Wieczór, A. Tobiszewski, P. Wityk, B. Tomiczek, and J. Czub, "Molecular Recognition in Complexes of TRF Proteins With Telomeric dna," *PLoS One* 9 (2014): e89460.

111. P. Dhungel, D. Brahim Belhaouari, and Z. Yang, "La-Related Protein 4 is Enriched in Vaccinia Virus Factories and is Required for Efficient Viral Replication in Primary Human Fibroblasts," *Microbiology Spectrum* 11 (2023): e01 390–23.

112. P. Chihomvu, A. Ganesan, S. Gibbons, K. Woollard, and M. A. Hayes, "Phytochemicals in Drug Discovery—A Confluence of Tradition and Innovation," *International Journal of Molecular Sciences* 25 (2024): 8792.

113. D. D. S. Nunes, L. M. Higa, R. L. Oliveira, et al., "In Vitro Susceptibility of Eighteen Clinical Isolates of Human Monkeypox Virus to Tecovirimat," *Memórias do Instituto Oswaldo Cruz* 118 (2023): e230056.